

Rapid *in situ* X-ray position stabilization via extremum seeking feedback

S. Zohar,* N. Venugopalan, D. Kissick, M. Becker, S. Xu, O. Makarov, S. Stepanov, C. Ogata, R. Sanishvili and R. F. Fischetti

Advanced Photon Source, Argonne National Laboratory, 9700 South Cass Avenue, BLDG 436, Argonne, IL 60439, USA.

*Correspondence e-mail: sioan@aps.anl.gov

Received 9 July 2015

Accepted 13 January 2016

Edited by P. A. Pianetta, SLAC National Accelerator Laboratory, USA

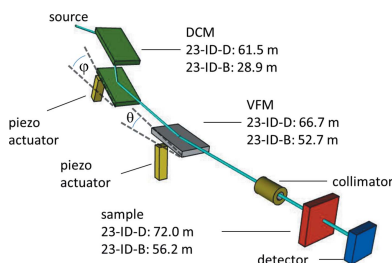
Keywords: extremum seeking; stabilization; feedback; X-rays.

X-ray beam stability is crucial for acquiring high-quality data at synchrotron beamline facilities. When the X-ray beam and defining apertures are of similar dimensions, small misalignments driven by position instabilities give rise to large intensity fluctuations. This problem is solved using extremum seeking feedback control (ESFC) for *in situ* vertical beam position stabilization. In this setup, the intensity spatial gradient required for ESFC is determined by phase comparison of intensity oscillations downstream from the sample with pre-existing vertical beam oscillations. This approach compensates for vertical position drift from all sources with position recovery times < 6 s and intensity stability through a $5\ \mu\text{m}$ aperture measured at 1.5% FWHM over a period of 8 hours.

1. Introduction

Synchrotron X-ray technology has shed light on a diverse array of fields extending from structural biology (Rasmussen *et al.*, 2007; Appelt *et al.*, 1981) and geology (Wenk *et al.*, 2000) to condensed matter (Mannini *et al.*, 2009; Bailey *et al.*, 2013; Rosenberg *et al.*, 2012; Zohar *et al.*, 2015) and chemistry (Qiao *et al.*, 2011; de Smit *et al.*, 2008). In recent years, interest in nanoscale phenomena has motivated significant effort to focus X-ray beams well below the micrometer level (Mimura *et al.*, 2009). Experiments exploiting such capabilities have been used to investigate the underlying behavior of magnetic vortex cores (Vansteenkiste *et al.*, 2009), verify integrated circuit integrity (Bajura *et al.*, 2011) and observe *in situ* nanometer-resolved spectroscopy of catalytic processes (de Smit *et al.*, 2008). For diffraction studies of nanoscale protein crystals with large unit cells, the conflicting demands on X-ray beam parameters complicate the situation. On the one hand, large unit cells require low beam divergence ($< 500\ \mu\text{rad}$) to resolve the tightly spaced diffraction peaks. On the other hand, achieving tightly focused beams capable of reducing background scattering by illuminating only the sample requires short focal length optics that increase beam divergence. To date, many beamlines balance these conflicting demands for both low divergence and tight focusing by using micrometer-scale collimators (Riekkel, 2000; Fischetti *et al.*, 2009; Xu *et al.*, 2011*a,b*), secondary source apertures (Hirata *et al.*, 2010) or a secondary pair of refocusing mirrors (Evans *et al.*, 2007).

Maintaining continuous alignment of micrometer-scale beams with micrometer-scale collimators is a challenging and time-consuming problem; when unaddressed it degrades both the intensity of the beam and the stability of the beam intensity. This is particularly detrimental for investigations of small, weakly scattering crystals of large protein complexes



© 2016 International Union of Crystallography

that require high signal-to-noise ratios for high-resolution structure refinement. Standard approaches for maintaining alignment use a combination of feedback from quadrant beam position monitors, automated beam positioning software and feedforward suppression of mechanical vibration, thermal fluctuations and electronic noise. These solutions, however, suffer from long-term drift due to nonlinearities in fluorescence detection, dark currents and hysteresis of piezo steering actuators. As both X-ray beam and defining aperture sizes continue to decrease, maintaining X-ray alignment will become an increasingly challenging endeavor.

In this article, we demonstrate an *in situ* extremum seeking feedback control for vertical beam position stabilization. Extremum seeking feedback (Krstic & Wang, 1999; Tan *et al.*, 2010) is a powerful control method that has found widespread applications ranging from wind turbine energy capture (Creaby *et al.*, 2009) and electro-inductive power transfer in plasmas (Carnevale *et al.*, 2009) to drag-lift optimization in fluids (King *et al.*, 2006) and stabilization of the intensity output from double-crystal monochromators (DCMs) (Fischetti *et al.*, 2004; Stoupin *et al.*, 2010; van Silfhout *et al.*, 2014; Mills & Pollock, 1980; van Mellaert & Schwuttke, 1970). Extremum seeking feedback control (ESFC) is a gradient-based optimization method that uses induced or naturally occurring perturbations modulating the control signal to estimate the system slope. With respect to DCM intensity stabilization, the slope indicates to which side of the second-crystal rocking curve the current position corresponds, and can be used to drive the second crystal towards the peak (Fischetti *et al.*, 2004; Stoupin *et al.*, 2010; van Silfhout *et al.*, 2014; Mills & Pollock, 1980; van Mellaert & Schwuttke, 1970). This is preferable in comparison with PID control which requires detuning the pitch of the DCM second crystal to the edge of the Bragg peak, where small changes in pitch of the second crystal can drive large intensity fluctuations. In this article, we demonstrate vertical position stabilization at the sample position using ESFC to steer a vertical focusing mirror (VFM) without introducing additional perturbation signals. We report intensity stability of 1.5% FWHM for duration of 8 h for a 5 μm beam with complete position recovery from introduced misalignments occurring within less than 6 s.

2. Theory

Despite the widespread implementation of ESFCs, rigorous proof for Hurwitz stability (Krstic & Wang, 1999) is a recent achievement with its effects still rippling throughout various disciplines. In the last decade, a minimalist approach using one integration stage without low- and high-pass filtering has been demonstrated (Tan *et al.*, 2010). Whereas the ESFC for the DCM second-crystal stabilization has a history of using digital lock-in amplifiers (LIAs) possessing built in tunable low-pass filters (LPFs) with time constants (TCs) of up to 30 ks (Fischetti *et al.*, 2004; Stoupin *et al.*, 2010), we analyze our system using the approach used by Tan *et al.* (2010), but with the single integration stage replaced with a LPF. The optical layout and control diagram for vertical positioning ESFC are

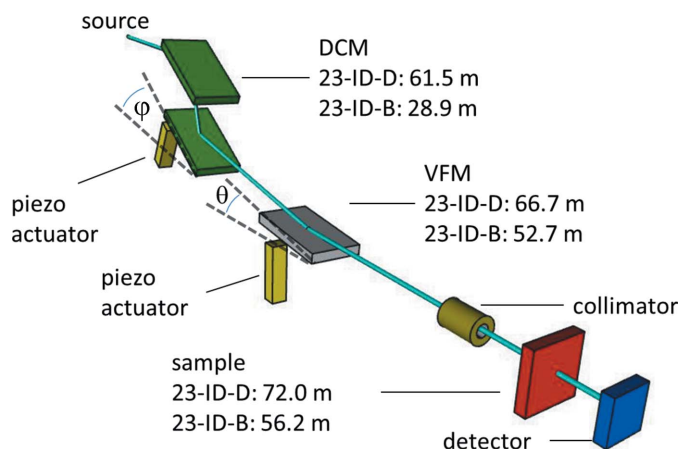


Figure 1
A narrow band of X-ray wavelengths is selected from the white beam using the DCM. The piezo actuator drives pitch oscillations in the second crystal at 198 Hz with estimated amplitudes of <30 nrad. These oscillations drive the beam position in and out of alignment with the collimator. The distances from the source have been labeled in the figure for each of the optical elements for both beamlines.

shown in Figs. 1 and 2, respectively. The modulation signal used for intensity stabilization drives the second-crystal monochromator pitch angle (φ) with response $\varphi' \sin(\omega t)$, where φ' is the pitch oscillation amplitude and ω is the modulation frequency. The pitch modulation of the second crystal not only oscillates the beam along the rocking curve enabling DCM intensity ESFC, but also introduces a small vertical position oscillation at the collimator located 30 mm upstream of the sample. This vertical position oscillation is equivalent to a VFM pitch oscillation with amplitude θ' , where

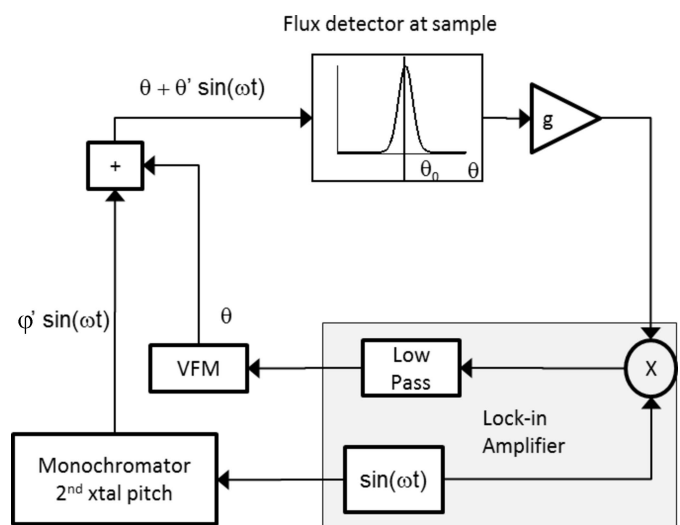


Figure 2
An excitation signal is applied to the DCM second crystal oscillating the beam along the DCM rocking-curve peak and vertically along the collimating optics immediately upstream of the sample and the detector. The phase is detected *via* the LIA and used to control the vertical VFM mirror piezo steering actuator. The lock-in here is phase locked with lock-in used for DCM feedback. Details for DCM lock-in feedback circuitry can be found in the literature (Fischetti *et al.*, 2004; Stoupin *et al.*, 2010; van Silfhout *et al.*, 2014; Mills & Pollock, 1980; van Mellaert & Schwuttke, 1970).

θ' can be obtained by taking the ratio of the vertical position oscillation amplitude at the collimator to the VFM–collimator distance. Further details regarding the collimator geometry are given by Fischetti *et al.* (2009) and Xu *et al.* (2011*a,b*). The intensity measured downstream from the aperture is amplified with gain (g) and channeled into an LIA. In the analysis presented here, all gain and attenuation stages are lumped into the gain term g . When the VFM steering angle θ is less than the optimal angle (θ_0) required to pass through the 5 μm collimator, beam intensity from vertical oscillations moving off the collimator are in phase with the modulation signal. When $\theta > \theta_0$, beam intensity from vertical oscillations moving off the collimator are π out of phase with the modulation signal. The LIA detects the phase change by multiplying the intensity signal from the sample with the modulating signal and detecting the DC component. This DC signal is fed back into the control of the piezo actuator that steers the VFM angle, centering the beam on the collimator. Simultaneous extremum seeking feedback for both monochromator flux and beam position at the collimator is achieved by synchronizing the LIA reference oscillators.

When the control signal delay and optical element TCs are sufficiently small, the resultant state space equation in the vicinity of a local maximum is

$$(\tau \text{d}/\text{d}t + 1)\theta = -gI[\theta + \theta' \sin(\omega t) - \theta_0]^2 \sin(\omega t), \quad (1)$$

where I is the beam intensity at the Bragg angle, τ is the LPF TC and t is time. The right-hand side of equation (1) is the input into the LPF, θ is proportional to the LPF output and the left-hand side term in parentheses is the differential form for low-pass filtering (Ogata, 2010). Expanding this expression yields

$$\tau \text{d}\theta/\text{d}t + \theta = gI[-(\omega - \omega_0)^2 \sin(\omega t) - \theta'^2 \sin^3(\omega t) - 2\theta'(\theta - \theta_0)^2 \sin^2(\omega t)]. \quad (2)$$

When the LPF cutoff $1/\tau \ll \omega$, the filter output components oscillating above ω have amplitudes several orders of magnitude less than frequency components below the cutoff. Thus, the first two terms on the right-hand side of equation (2) can be neglected. Similarly, expanding $\sin^2(\omega t)$ into $[1 - \sin(2\omega t)]/2$ and neglecting the oscillating terms yields

$$\tau \text{d}\theta/\text{d}t + \theta = -gI\theta'(\theta - \theta_0). \quad (3)$$

A more rigorous justification for such approximations using singular perturbation theory to separate out dynamics at different timescales is given by Krstic & Wang (1999) and Tan *et al.* (2010). Equation (3) is an ordinary differential equation with impulse response

$$\theta = \theta_i \exp(\lambda t) + \theta_0, \quad (4)$$

where θ_i is a small impulse and the characteristic polynomial is $\lambda = -(1 + gI\theta')/\tau$. In this approximation, the system exponentially converges towards the maximum. In practice, additional system TCs, response delays and large deviations introduce higher-order differential, delay differential and nonlinear terms, respectively, into equation (1). These terms

increase characteristic polynomial order to greater than two and introduce transcendental and nonlinear terms. Thus, the Routh–Hurwitz stability condition requiring all roots of λ to have real components less than zero is not guaranteed. The equation for DCM feedback is similarly derived by replacing the VFM steering angle θ with the DCM pitch angle φ .

3. Results

In this section, we present our results for ESFC of monochromator intensity and vertical position. Experiments were conducted at the Advanced Photon Source at GM/CA-XSD, beamlines 23-ID-D and 23-ID-B. In Figs. 3(*a*) and 3(*c*), the DCM intensity response to small impulses that misalign the DCM second-crystal pitch acquired on beamline 23-ID-B at 12 keV are shown. Increasing the LPF TC and sensitivity (*i.e.* inverse gain) increases the time required for convergence to the stability value. The responses are not purely exponential, due to amplifier saturation upon large deviation from the extremum. As the system nears alignment, however, the responses become exponential permitting least-squares fitting. The fitted convergence times are plotted with respect to the sensitivity and LPF TC and shown in Figs. 3(*b*) and 3(*d*). The convergence time dependencies on both the LPF TC and sensitivity are well fitted by a power law with an exponent of 0.35. The common exponent value of 0.35 shared in both LPF TC and sensitivity convergence time dependencies indicates the convergence time depends on the product of the LPF TC with sensitivity in agreement with the equations above. The fact that the exponent is not 1 indicates the system under control possesses a characteristic polynomial of order > 2 .

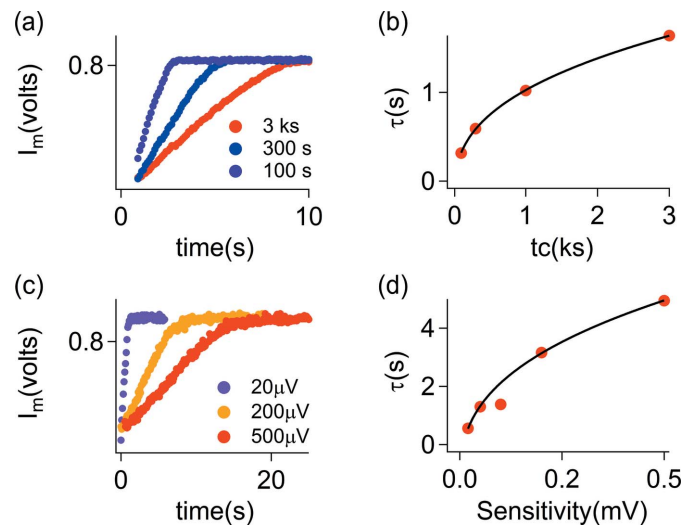


Figure 3 The DCM output intensity (I_m) stabilization feedback system temporal response to DCM second crystal deflection for varying TC and gain parameters are shown in panels (*a*) and (*c*). In panel (*a*) the sensitivity is fixed at 5 mV and the LPF TC is varied. The convergence time dependence on the LPF TC is shown in panel (*b*). In panel (*c*) the LPF TC is fixed at 3 ks (and the sensitivity is varied). The convergence time dependence on the sensitivity is shown in panel (*d*).

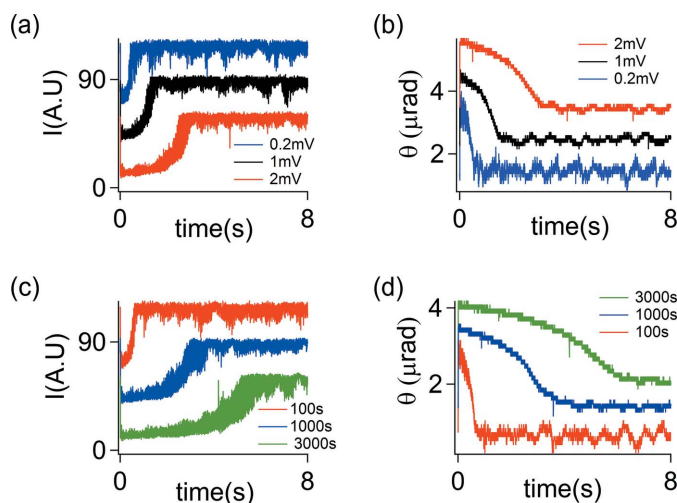


Figure 4 Positional feedback response to impulse deflections of the VFM steering angle; dependence on sensitivity and LPF TC taken at 13.6 keV for the active beam stop intensity (a, c) and VFM piezo steering actuator voltage (b, d). Increasing the TC and increasing the gain decreases the settling time at the cost of long-term oscillations. The steps in the VFM angle response in panels (b) and (d) are due to the finite resolution of the scaler and voltage-to-frequency instrumentation used to record the VFM piezo readback voltage. Data presented in these graphs have been offset for clarity.

In Fig. 4, we show the vertical positioning ESFC acquired on beamline 23-ID-B on timescales of several seconds at 13.6 keV for impulses applied to the VFM piezo steering actuator. Intensity detection in these measurements was achieved using an X-ray sensitive beam stop (Xu *et al.*, 2010) that measures the X-ray photoemission current between a coaxial molybdenum rod and tube separated by an insulating Kapton tube and subject to a 50 V bias. After the initial jump, the intensity and VFM steering actuator converge towards the stability value at rates dependent on the TC and sensitivity settings. Whereas the convergence time monotonically depends on the TC and sensitivity, the noise in the impulse response near the extremum is too large to permit fitting with an exponential. The impulses knock the beam out of alignment such that up to 85% of intensity may be lost. Once the peak has been reached, oscillations with time constant and amplifier-gain-dependent amplitudes appear in the VFM piezo steering actuator voltage, with larger amplitude oscillations coinciding with faster convergence times.

In Fig. 5, we show the feedback performance data acquired on beamline 23-ID-D on timescales greater than 8 h using a diode detector instead of an active beam stop. The intensity stability over this duration is 1.5% FWHM. The VFM piezo steering actuator voltage compensates 17.6 μm of thermally induced beam drift originating from a large energy change immediately prior to measurements. The large intensity drops of up to $\sim 50\%$ are attributed to particle beam perturbations from injections during top-up mode, and occur over 90% less frequently when not in top-up mode. A histogram of the intensities is shown in the inset of Fig. 5. The asymmetric shape of the distribution is on account of the intensity which

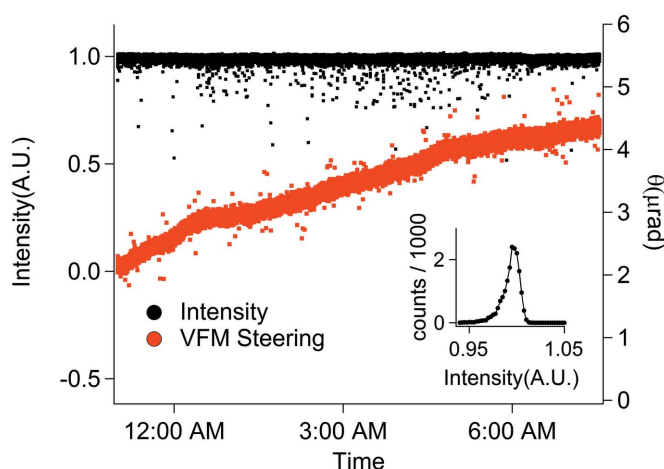


Figure 5 Simultaneous positional and DCM intensity ESFC with beam intensity measured through a 5 μm collimator for an 8 h duration. The black points are the intensity through the collimator and the red points are the VFM steering angle. The inset shows a histogram of the beam intensity at the sample over the 8 h period. The full width at half-maximum to mean ratio is 1.5% throughout this duration. Experimental parameters for position feedback were 12 keV, 30000 s TC, 2 mV sensitivity and <30 nrad modulation amplitude.

can never exceed the maximum intensity that occurs with optimal beam-collimator alignment.

Vertical position oscillation amplitudes of $0.2 \pm 0.1 \mu\text{m}$ were measured by taking the difference between vertical beam widths at the collimator, measured with DCM second-crystal pitch oscillations present and not present. This value is substantially smaller than the 28 μm vertical beam width and is expected to introduce $<0.02\%$ intensity oscillation downstream from the collimator at the first-harmonic frequency (396 Hz), assuming a Gaussian-shaped beam. This measured vertical position oscillation amplitude would require a DCM second-crystal pitch modulation of $\phi' < 30$ nrad. Our estimate for the pitch modulation of the second crystal is substantially less than the measured 30 μrad rocking curve FWHM for Si (111) at 12 keV. Modulation amplitudes of this order introduce $<0.01\%$ intensity fluctuations immediately downstream from the DCM at the first-harmonic frequency, assuming a Gaussian-shaped rocking curve.

In addition to beam stabilization, this ESFC approach also provides the ability to track collimator motion in the vertical direction. Furthermore, the intensity detector is not restricted to a transmission detector or intensity-sensitive beam stop, but can also be the photoemission drain current from the sample itself.

4. Conclusion

In conclusion, we have extended extremum seeking feedback used for DCM intensity stabilization to vertical position stabilization by controlling the VFM piezo actuator voltage without introducing additional perturbation signals. This feedback technique maintains the beam at optimal alignment for a duration of 8 h with a noise profile of 1.5% FWHM.

Feedback recovery from impulses applied to the VFM piezo actuator is less than 6 s. Finally, we note that the presence of a perturbation signal from which the position gradient was extracted is serendipitous. If other phase-stable beam oscillations originating upstream from the monochromator in the synchrotron accelerator exist, they could be similarly exploited for ESFC optimization of: (1) the DCM second-crystal Bragg angle, (2) vertical positioning and (3) horizontal positioning without introducing vibrations in the second crystal of the DCM.

Acknowledgements

Work at the Argonne National Laboratory was supported through interagency agreement with the US National Institutes of Health under US Department of Energy contract DE-AC02-06CH11357.

References

- Appelt, K., Dijk, J., Reinhardt, R., Sanhuesa, S., White, S. W., Wilson, K. S. & Yonath, A. (1981). *J. Biol. Chem.* **256**, 11787–11790.
- Bailey, W. E., Cheng, C., Knut, R., Karis, O., Auffret, S., Zohar, S., Keavney, D., Warnicke, P., Lee, J. S. & Arena, D. A. (2013). *Nat. Commun.* **4**, 2025.
- Bajura, M., Boverman, G., Tan, J., Wagenbreth, G., Rogers, C. M., Feser, M., Rudati, J., Tkachuk, A., Aylward, S. & Reynolds, P. (2011). *Proceedings of the 36th GOMACTech Conference*, Orlando, FL, USA, 21–24 March 2011.
- Carnevale, D., Astolfi, A., Centioli, C., Podda, S., Vitale, V. & Zaccarian, L. (2009). *Fusion Eng. Des.* **84**, 554–558.
- Creaby, J., Li, Y. & Seem, J. (2009). *Wind Eng.* **33**, 361–387.
- Evans, G., Alianelli, L., Burt, M., Wagner, A. & Sawhney, K. J. S. (2007). *AIP Conf. Proc.* **879**, 836–839.
- Fischetti, R., Stepanov, S., Rosenbaum, G., Barrea, R., Black, E., Gore, D., Heurich, R., Kondrashkina, E., Kropf, A. J., Wang, S., Zhang, K., Irving, T. C. & Bunker, G. B. (2004). *J. Synchrotron Rad.* **11**, 399–405.
- Fischetti, R. F., Xu, S., Yoder, D. W., Becker, M., Nagarajan, V., Sanishvili, R., Hilgart, M. C., Stepanov, S., Makarov, O. & Smith, J. L. (2009). *J. Synchrotron Rad.* **16**, 217–225.
- Hirata, K., Ueno, G., Nisawa, A., Kawano, Y., Hikima, T., Shimizu, N., Kumasaka, T., Yumoto, H., Tanaka, T., Takahashi, S. & Ohashi, H. (2010). *AIP Conf. Proc.* **1234**, 901–904.
- King, R., Becker, R., Feuerbach, G., Henning, L., Petz, R., Nitsche, W., Lemke, O. & Neise, W. (2006). *Proceedings of the 14th Mediterranean Conference on Control and Automation (Med'06)*, pp. 1–6.
- Krstic, M. & Wang, H.-H. (1999). *Automatica*, **36**, 595.
- Mannini, M., Pineider, F., Sainctavit, P., Danieli, C., Otero, E., Sciancalepore, C., Talarico, A. M., Arrio, M. A., Cornia, A., Gatteschi, D. & Sessoli, R. (2009). *Nat. Mater.* **8**, 194–197.
- Mellaert, L. J. van & Schwuttke, G. H. (1970). *Phys. Status Solidi A*, **3**, 687–696.
- Mills, D. & Pollock, V. (1980). *Rev. Sci. Instrum.* **51**, 1664–1668.
- Mimura, H., Handa, S., Kimura, T., Yumoto, H., Yamakawa, D., Yokoyama, H., Matsuyama, S., Inagaki, K., Yamamura, K., Sano, Y., Tamasaku, K., Nishino, Y., Yabashi, M., Ishikawa, T. & Yamauchi, K. (2009). *Nat. Phys.* **6**, 122–125.
- Ogata, K. (2010). *Modern Control Engineering*, 5th ed. Boston: Prentice-Hall.
- Qiao, B., Wang, A., Yang, X., Allard, L. F., Jiang, Z., Cui, Y., Liu, J., Li, J. & Zhang, T. (2011). *Nat. Chem.* **3**, 634–641.
- Rasmussen, S. G. F., Choi, H., Rosenbaum, D. M., Kobilka, T. S., Thian, F. S., Edwards, P. C., Burghammer, M., Ratnala, V. R. P., Sanishvili, R., Fischetti, R. F., Schertler, G. F. X., Weis, W. I. & Kobilka, B. K. (2007). *Nature (London)*, **450**, 383–387.
- Riekell, C. (2000). *Rep. Prog. Phys.* **63**, 233–262.
- Rosenberg, R. A., Zohar, S., Keavney, D., Divan, R., Rosenmann, D., Mascarenhas, A. & Steiner, M. A. (2012). *Rev. Sci. Instrum.* **83**, 073701.
- Silfhout, R. van, Kachatkou, A., Groppo, E., Lamberti, C. & Bras, W. (2014). *J. Synchrotron Rad.* **21**, 401–408.
- Smit, E. de, Swart, I., Creemer, J. F., Hoveling, G. H., Gilles, M. K., Tyliczszak, T., Kooyman, P. J., Zandbergen, H. W., Morin, C., Weckhuysen, B. M. & de Groot, F. M. (2008). *Nature (London)*, **456**, 222–225.
- Stoupin, S., Lenkszus, F., Laird, R., Goetze, K., Kim, K. J. & Shvyd'ko, Y. (2010). *Rev. Sci. Instrum.* **81**, 055108.
- Tan, Y., Moase, W. H., Manzie, C., Nestic, D. & Mareels, I. M. Y. (2010). *Proceedings of the 29th Chinese Control Conference*, Beijing, China, 29–31 July 2010, pp. 14–26.
- Vansteenkiste, A., Chou, K. W., Weigand, M., Curcic, M., Sackmann, V., Stoll, H., Tyliczszak, T., Woltersdorf, G., Back, C. H., Schütz, G. & Van Waeyenberge, B. (2009). *Nat. Phys.* **5**, 332–334.
- Wenk, H.-R., Matthies, S., Hemley, R. J., Mao, H.-K. & Shu, J. (2000). *Nature (London)*, **405**, 1044–1047.
- Xu, S., Keefe, L. J., Mulichak, A., Yan, L., Alp, E. E., Zhao, J. & Fischetti, R. F. (2011a). *Nucl. Instrum. Methods Phys. Res. A*, **649**, 104–106.
- Xu, S., Nagarajan, V., Sanishvili, R. & Fischetti, R. F. (2011b). *Proc. SPIE*, **8125**, 81250X.
- Xu, S., Makarov, O., Benn, R., Yoder, D. W., Stepanov, S., Becker, M., Corcoran, S., Hilgart, M., Nagarajan, V., Ogata, C. M., Pothineni, S., Sanishvili, R., Smith, J. L., Fischetti, R. F., Garrett, R., Gentle, I., Nugent, K. & Wilkins, S. (2010). *AIP Conf. Proc.* **1234**, 905–908.
- Zohar, S., Choi, Y., Love, D. M., Mansell, R., Barnes, C. H. W., Keavney, D. J. & Rosenberg, R. A. (2015). *Appl. Phys. Lett.* **106**, 072408.